Temporal Image Reconstruction in Electrical Impedance Tomography

Andy Adler[1], Tao Dai[1], William R.B. Lionheart[2]

[1] Systems and Computer Engineering, Carleton University, Ottawa, Canada
[2] School of Mathematics, University of Manchester, UK

E-mail: `adler@sce.carleton.ca`

Abstract. Electrical Impedance Tomography (EIT) calculates images of the body from body impedance measurements. While the spatial resolution of these images is relatively low, the temporal resolution of EIT data can be high. Most EIT reconstruction algorithms solve each data frame independently, although Kalman filter algorithms track the image changes across frames. This paper proposes a new approach which directly accounts for correlations between images in successive data frames. Image reconstruction is posed in terms of an augmented image $\tilde{\mathbf{x}}$ and measurement vector $\tilde{\mathbf{y}}$, which concatenate the values from the d previous and future frames. Image reconstruction is then based on an augmented regularization matrix $\tilde{\mathbf{R}}$, which accounts for a model of both the spatial and temporal correlations between image elements. Results are compared for reconstruction algorithms based on independent frames, Kalman filters, and the proposed approach. For low values of the regularization hyperparameter, the proposed approach performs similarly to independent frames, but for higher hyperparameter values, it uses adjacent frame data to reduce reconstructed image noise.

Keywords: Electrical Impedance Tomography, regularization, image reconstruction,

1. Introduction

Electrical Impedance Tomography (EIT) calculates an estimate of the conductivity distribution within a body based on current stimulations and voltage measurements on the body surface. EIT has fairly low spatial resolution, limited by the low sensitivity of surface measurements to conductivity changes deep within the body. On the other hand, EIT has excellent temporal resolution, with some recent systems having frame rates up to 1000/s (Wilkinson et al 2005). Such high temporal resolution makes EIT a promising technology to monitor fast physiological events which affect the conductivity distribution. For cardiac activity, the frequency content of the QRS complex is mainly between 10–25 Hz (Kohler et al 2002). Another example is high frequency ventilation in which air is pumped into the lungs at rates of 5–25 Hz (with smaller tidal volumes). High frequency ventilation is indicated for many patients with respiratory distress syndrome since it is understood to place less stress on injured lung tissue (Eichenwald, 1999). EIT can potentially be of great benefit to these patients, since the distribution of ventilation

in their lungs is highly non-uniform and cannot be otherwise monitored (Wolf and Arnold, 2005).

Like many biomedical instrumentation techniques, the ability of EIT to see small physiological changes is limited by the signal to noise ratio (SNR). A widely used technique to improve SNR is ensemble averaging, which reduces random noise by the square root of the number of averaged frames. If EIT data acquisition is sufficiently rapid compared to the underlying physiological processes to be imaged, then ensemble averaging may be used on multiple frames of EIT. However, in EIT applications where conductivity changes are very fast with respect to the EIT frame rate, ensemble averaging is not appropriate, since it will effectively reduce the temporal resolution. In these cases, each frame of EIT data is typically reconstructed independently of the others.

In this paper, we are interested in approaches to image a body which is undergoing fast changes with respect to the EIT frame rate. In these cases, ensemble averaging is not appropriate; however, it is clear that individual data frames are not completely independent, but do contain useful correlations, which could be exploited to improve EIT image noise performance. We call an approach which uses the time sequence of EIT frame data *temporal image reconstruction.*

Temporal image reconstruction can be represented as a linear tracking problem, and formulated as an extended Kalman filter, in which the image at each instant is estimated from the current data and the previous image estimate. Vauhkonen et al (1998a) proposed the first Kalman filter based algorithm for difference EIT; we describe this approach using the notation of this paper in section 2.3. More recently, this approach has been extended by Kim et al (2004) to reconstruct the resistivity of a contrast of known shape and location. Kim et al (2006) also proposed a computationally efficient algorithm based on pre-computing the Kalman gain and state estimation matrices. An algorithm for absolute EIT has also been shown for simulation data (Trigo et al 2004).

In this paper, we propose a new approach for temporal EIT image reconstruction, which directly estimates the image at frame t_0 from the set of data in a window of frames from t_{-d} to t_d. Using these data, the temporal inverse is formulated as an inverse problem with a regularization prior which accounts for both spatial and temporal correlations between image elements.

2. Methods

We consider an EIT system with n_E electrodes applied to a body using sequential current stimulation with parallel voltage measurement. Using these electrodes, n_E current stimulation patterns are sequentially applied and n_V differential measurements are made for each stimulation. For an adjacent drive EIT system, voltages are typically not measured at driven electrodes, and $n_V = n_E - 3$. The delay between each successive stimulation pattern is t_S; thus, a complete set (frame) of EIT measurements takes time $t_F = n_E t_S$. Each data frame measures a vector, $\mathbf{v} \in \mathbb{R}^{n_M}$, of $n_M = n_E n_V$ data

points (some of which are redundant if the medium is not changing). Difference EIT calculates difference data $\mathbf{y}$, ($[\mathbf{y}]_i = [\mathbf{v}_2]_i - [\mathbf{v}_1]_i$; or the normalized difference data $[\mathbf{y}]_i = ([\mathbf{v}_2]_i - [\mathbf{v}_1]_i)/[\mathbf{v}_1]_i$). To improve its precision, $\mathbf{v}_1$ is typically averaged over many data frames, at a time when the conductivity distribution may be assumed to be stable; we thus assume that $\mathbf{v}_1$ is noise free.

The body under investigation is modelled using a finite element model (FEM) which discretizes the conductivity onto n_N piecewise smooth elements, represented by a vector $\boldsymbol{\sigma} \in \mathbb{R}^{n_N}$ (In this paragraph, $\boldsymbol{\sigma}$ represents conductivity; elsewhere in this paper, σ is the standard deviation). Again, difference EIT calculates a vector of conductivity change, $\mathbf{x} = \boldsymbol{\sigma}_2 - \boldsymbol{\sigma}_1$ between the present conductivity distribution, $\boldsymbol{\sigma}_2$, and that at the reference measurement, $\boldsymbol{\sigma}_1$. For small variations around the reference conductivity $\boldsymbol{\sigma}_1$, the relationship between $\mathbf{x}$ and $\mathbf{y}$ can be linearized (giving the difference EIT forward model):

$$\mathbf{y} = \mathbf{J}\mathbf{x} + \mathbf{n} \tag{1}$$

where $\mathbf{J} \in \mathbb{R}^{n_M \times n_N}$ is the Jacobian or sensitivity matrix and $\mathbf{n} \in \mathbb{R}^{n_M}$ is the measurement noise which is assumed to be uncorrelated white Gaussian. $\mathbf{J}$ is calculated from the FEM as $\mathbf{J}_{ij} = \left.\frac{\partial \mathbf{y}_i}{\partial \mathbf{x}_j}\right|_{\boldsymbol{\sigma}_1}$, and depends on the FEM, current injection patterns, the reference conductivity, and the electrode models. This system is underdetermined since $n_N > n_M$. This problem is commonly solved using regularization techniques (eg. Cheney et al 1990, Adler and Lionheart, 2006) in order to calculate a conductivity change estimate, $\hat{\mathbf{x}}$, which is both faithful to the measurements, $\mathbf{y}$, and to *a priori* constraints on a "reasonable" image.

Over time steps, k, a sequence of difference vectors, $\mathbf{y}_k = \mathbf{J}\mathbf{x}_k$, are measured (assuming the body and electrode geometry, and thus $\mathbf{J}$, stay fixed). If the conductivity of the body under investigation doesn't change too rapidly, then it is reasonable to expect that a certain number of measurements, d, into the past and future provide useful information about the current image. Labelling the current instant as t, we therefore seek to estimate $\hat{\mathbf{x}}_t$ from data $[\mathbf{y}_{t-d}; \ldots; \mathbf{y}_{t-1}; \mathbf{y}_t; \mathbf{y}_{t+1}; \ldots; \mathbf{y}_{t+d}]$.

In the subsequent sections we consider three traditional approaches and the proposed *temporal inverse*; each estimates $\hat{\mathbf{x}}_t$ at frame t from a sequence of data starting at frame 0, using the indicated data: 2.1) *Gauss-Newton (GN) inverse*, using $\mathbf{y}_t$ only; 2.2) *GN with weighted data*, using a weighted average of $\mathbf{y}_{t-d} \ldots \mathbf{y}_{t+d}$; 2.3) *Kalman filter inverse*, using all previous and current data, $\mathbf{y}_0 \ldots \mathbf{y}_t$; and 2.4) *Temporal inverse*, using $\mathbf{y}_{t-d} \ldots \mathbf{y}_{t+d}$ based on a temporal prior model.

2.1. One-step linear GN(Gauss-Newton) solver

One-step Gauss-Newton (GN) EIT reconstruction approaches have been widely used in EIT (eg. Cheney et al 1990; Adler and Guardo, 1996). They allow use of sophisticated regularized models of the EIT inverse problem, are able to represent this solution as a linear reconstruction matrix, which can then allow rapid, real-time imaging. The GN inverse problem seeks to calculate a solution, $\hat{\mathbf{x}}$, to the EIT inverse problem expressed

as the minimum of a sum of quadratic norms

$$\|\mathbf{y} - \mathbf{J}\hat{\mathbf{x}}\|^2_{\Sigma_n^{-1}} + \|\mathbf{x} - \mathbf{x}^\circ\|^2_{\Sigma_x^{-1}} \tag{2}$$

where $\mathbf{x}^\circ$ represents the expected value of element conductivity changes, which is zero for difference EIT. $\Sigma_n \in \mathbb{R}^{n_M \times n_M}$ is the covariance matrix of the measurement noise $\mathbf{n}$. Since $\mathbf{n}$ is uncorrelated, Σ_n is a diagonal matrix with $[\Sigma_n]_{i,i} = \sigma_i^2$, where σ_i^2 is the noise variance at measurement i. $\Sigma_x \in \mathbb{R}^{n_N \times n_N}$ is the expected image covariance.

Typically, Σ_n and Σ_x are not calculated directly. Instead, their inverses, $\mathbf{W} = \sigma_n^2 \Sigma_n^{-1}$ and $\mathbf{R} = \sigma_x^2 \Sigma_x^{-1}$, are heuristically determined from *a priori* considerations. Here σ_n is the average measurement noise amplitude and σ_x is the *a priori* amplitude of conductivity change. $\mathbf{W}$ models the measurement accuracy. For uncorrelated noise, each diagonal element is proportional to the signal to noise ratio. For difference EIT with identical channels, $\mathbf{W} = \mathbf{I}$. The regularization matrix $\mathbf{R}$ may be understood to model the "unlikelihood" of image elements.

By solving (2), a linearized, one-step inverse solution is obtained as

$$\hat{\mathbf{x}} = \left(\mathbf{J}^T \frac{1}{\sigma_n^2} \mathbf{W} \mathbf{J} + \frac{1}{\sigma_x^2} \mathbf{R}\right)^{-1} \mathbf{J}^T \frac{1}{\sigma_n^2} \mathbf{W} \mathbf{y} \tag{3}$$

We define the hyperparameter $\lambda = \sigma_n / \sigma_x$, and rewrite (3) as

$$\hat{\mathbf{x}} = \left(\mathbf{J}^T \mathbf{W} \mathbf{J} + \lambda^2 \mathbf{R}\right)^{-1} \mathbf{J}^T \mathbf{W} \mathbf{y} = \mathbf{B} \mathbf{y} \tag{4}$$

where $\mathbf{B} = \left(\mathbf{J}^T \mathbf{W} \mathbf{J} + \lambda^2 \mathbf{R}\right)^{-1} \mathbf{J}^T \mathbf{W}$ is the linear, one-step inverse. The regularization hyperparameter λ controls the trade-off between resolution and noise attenuation in the reconstructed image.

If image elements are assumed to be independent with identical expected magnitude, $\mathbf{R}$ becomes an identity matrix $\mathbf{I}$ and (4) uses zeroth-order Tikhonov regularization. For EIT, such solutions tend to push reconstructed noise toward the boundary, since the measured data are much more sensitive to boundary image elements. Instead, $\mathbf{R}$ may be scaled with the sensitivity of each element, so that each diagonal element i of $\mathbf{R}$ is $[\mathbf{R}]_{i,i} = \left[\mathbf{J}^T \mathbf{J}\right]^p_{i,i}$. This is the NOSER prior of Cheney et al (1990) for an exponent $p = 1$. Many other prior matrices have been proposed: to model image smoothness as a penalty for non-smooth image regions, $\mathbf{R}$ may be set to the discrete Laplacian filter (Vauhkonen, 1998b) or a discrete high pass Gaussian filter (Adler and Guardo, 1996).

In this paper, the NOSER prior is used for calculating the matrix $\mathbf{R}$ with $p = 0.5$ in all tested algorithms, except for the Kalman filtering. Because it is diagonal, $\mathbf{R}$ can be inverted without numerical difficulties. The choice of exponent is a heuristic compromise between the pushing noise to the boundary ($p = 0$) or to the centre ($p = 1$).

In (4), the term in the inverse is of size $n_N \times n_N$. To save computational time, and improve inverse accuracy and stability, we want to decrease the size of the matrix to be

inverted. Thus, we rewrite the matrix $\mathbf{B}$ using the *data form* as:

$$
= \left(\mathbf{J}^T \mathbf{W} \mathbf{J} + \lambda^2 \mathbf{R}\right)^{-1} \mathbf{J}^T \mathbf{W} \left[\left(\mathbf{J}\frac{1}{\lambda^2}\mathbf{P}\mathbf{J}^T + \mathbf{V}\right)\left(\mathbf{J}\frac{1}{\lambda^2}\mathbf{P}\mathbf{J}^T + \mathbf{V}\right)^{-1}\right]
$$

$$
= \left(\mathbf{J}^T \mathbf{W} \mathbf{J} + \lambda^2 \mathbf{R}\right)^{-1} \left(\mathbf{J}^T \mathbf{W} \mathbf{J} + \lambda^2 \mathbf{R}\right)\left(\frac{1}{\lambda^2}\mathbf{P}\mathbf{J}^T\right)\left(\mathbf{J}\frac{1}{\lambda^2}\mathbf{P}\mathbf{J}^T + \mathbf{V}\right)^{-1}
$$

$$
= \mathbf{P}\mathbf{J}^T \left(\mathbf{J}\mathbf{P}\mathbf{J}^T + \lambda^2 \mathbf{V}\right)^{-1} \tag{5}
$$

where $\mathbf{P} = \mathbf{R}^{-1} = \frac{1}{\sigma_x^2}\Sigma_x$ and $\mathbf{V} = \mathbf{W}^{-1} = \frac{1}{\sigma_n^2}\Sigma_n$. In practice, $\mathbf{P}$ and $\mathbf{V}$ are modelled directly from the system covariances, rather than the inverse of $\mathbf{R}$ and $\mathbf{W}$. Using (5), the size of the term in the inverse is reduced to $n_M \times n_M$. This is especially significant for 3D EIT models and for the temporal inverse which we introduce below.

Note that the GN solver does not consider the time sequence of EIT data. Each frame is solved individually, and inter-frame correlations are ignored.

2.2. One-step linear GN solver with weighted data

The one-step linear GN solver may be applied to weighted average data in order to implement ensemble averaging. Given a temporal window with a half width d, we model the time constant, τ, to represent the rate at which the most rapid changes of interest occur in the body. That means that a feature of interest in a frame will dissipate by a factor of $\gamma = \exp(-t_F/\tau)$ in the next frame, and by γ^d in the dth subsequent frame. Using this factor, we calculate a weighted ensemble average EIT measurement, $\bar{\mathbf{y}}$

$$
\bar{\mathbf{y}} = \frac{1}{w_\gamma}\sum_{i=-d}^{d}\gamma^{|i|}\mathbf{y}_i \tag{6}
$$

where $w_\gamma = \sum_{i=-d}^{d}\gamma^{|i|}$. When $0 < \gamma < 1$, this is a forgetting process, and when $\gamma = 1$, an averaging process. Noise amplitude will decrease by a factor of $\sqrt{w_\gamma}$ due to this ensemble averaging. The GN solver with weighted data reconstructs images as

$$
\hat{\mathbf{x}} = \mathbf{B}\bar{\mathbf{y}} \tag{7}
$$

where $\mathbf{B}$ is calculated using (4).

2.3. Kalman solver

The Kalman filter is a widely used approach for many tracking and data prediction tasks. The EIT image reconstruction algorithm of Vauhkonen et al (1998a) is formulated as an iterative state estimation problem. The system discrete time *prediction model* is given by (using the notation introduced above)

$$
\mathbf{x}_k = \mathbf{A}\mathbf{x}_{k-1} + \mathbf{v} \tag{8}
$$

for a discrete time sequence k. $\mathbf{A} \in \mathbb{R}^{n_N \times n_N}$ is the state transition matrix, and $\mathbf{v} \in \mathbb{R}^{n_N}$ is the state noise (assumed to be zero mean white Gaussian). One traditional difficulty

with Kalman filters is finding values for state space parameters. If the underlying processes in the body were well known, then $\mathbf{A}$ could be derived; for example, in a stirred mixing tank, the process would rotate image elements in each frame. We follow the traditional heuristic approach of assigning $\mathbf{A} = \mathbf{I}$ (representing a random walk process) and setting the state noise covariance to the image element covariance $\mathbf{P}$. The discrete time *observation model* at time step k is:

$$\mathbf{y}_k = \mathbf{J}_k \mathbf{x}_k + \mathbf{n} \tag{9}$$

which is equivalent to (1) if $\mathbf{J}$ is constant. Kalman image reconstruction iteratively estimates $\mathbf{x}_k$ based on the previous image $\mathbf{x}_{k-1}$ and measurements $\mathbf{y}_k$.

$$\mathbf{x}_k^- = \mathbf{A}\hat{\mathbf{x}}_{k-1} \qquad\qquad \text{\textit{state estimation}} \tag{10}$$

$$\hat{\mathbf{x}}_k = \mathbf{x}_k^- + \mathbf{K}_k(\mathbf{y}_k - \mathbf{J}_k \mathbf{x}_k^-) \quad \text{\textit{state correction}} \tag{11}$$

where $\mathbf{K}_k$ is the Kalman gain, which is calculated from the error covariance estimate $\mathbf{C}_k$ as:

$$\mathbf{C}_k^- = \mathbf{A}\hat{\mathbf{C}}_{k-1}\mathbf{A}^T + \mathbf{P} \qquad\qquad \text{\textit{error covariance estimation}} \tag{12}$$

$$\mathbf{K}_k = \mathbf{C}_k^- \mathbf{J}_k^T \left(\mathbf{J}_k \mathbf{C}_k^- \mathbf{J}_k^T + \mathbf{V}\right)^{-1} \quad \text{\textit{Kalman gain}} \tag{13}$$

$$\hat{\mathbf{C}}_k = (\mathbf{I} - \mathbf{K}_k \mathbf{J}_k)\,\mathbf{C}_k^- \qquad\qquad \text{\textit{error covariance correction}} \tag{14}$$

Iterative calculation of $\mathbf{K}$ is computationally expensive. If $\mathbf{J}$ is constant, $\mathbf{K}$ will eventually stabilize, and may be precomputed (Kim et al 2006) in order to dramatically speed up the calculation. We do not take this approach here.

2.4. Temporal one-step solver

Instead of calculating an image based on the sequence of past frames, we propose a temporal image reconstruction algorithm which uses a set of data frames nearby in time. The data frame sequence is treated as a single inverse problem, with a regularization prior to account for both spatial and temporal correlations between image elements. Given a vertically concatenated sequence of measurements frames $\tilde{\mathbf{y}}_t = [\mathbf{y}_{t-d}; \ldots; \mathbf{y}_t; \ldots; \mathbf{y}_{t+d}]$ and the corresponding concatenated images $\tilde{\mathbf{x}}_t = [\mathbf{x}_{t-d}; \ldots; \mathbf{x}_t; \ldots; \mathbf{x}_{t+d}]$, the direct temporal forward model (1) is rewritten as

$$
\begin{bmatrix} \mathbf{y}_{t-d} \\ \vdots \\ \mathbf{y}_t \\ \vdots \\ \mathbf{y}_{t+d} \end{bmatrix}
=
\begin{bmatrix} \mathbf{J} & & \cdots & & 0 \\ & \ddots & & & \\ \vdots & & \mathbf{J} & & \vdots \\ & & & \ddots & \\ 0 & & \cdots & & \mathbf{J} \end{bmatrix}
\begin{bmatrix} \mathbf{x}_{t-d} \\ \vdots \\ \mathbf{x}_t \\ \vdots \\ \mathbf{x}_{t+d} \end{bmatrix}
+
\begin{bmatrix} \mathbf{n}_{t-d} \\ \vdots \\ \mathbf{n}_t \\ \vdots \\ \mathbf{n}_{t+d} \end{bmatrix}
\tag{15}
$$

and also as

$$\tilde{\mathbf{y}}_t = \tilde{\mathbf{J}}\tilde{\mathbf{x}}_t + \tilde{\mathbf{n}}_t \tag{16}$$

where $\tilde{\mathbf{n}}_t = [\mathbf{n}_{t-d}; \ldots; \mathbf{n}_t; \ldots; \mathbf{n}_{t+d}]$. We assume $\mathbf{J}$ to be constant, although this formulation could be modified to account for a time varying $\mathbf{J}$. Based on this approximation $\tilde{\mathbf{J}} = \mathbf{I} \otimes \mathbf{J}$, where the identity matrix $\mathbf{I}$ has size $2d + 1$, and $\otimes$ is the Kronecker product.

The correlation of corresponding elements between adjacent frames (delay $\delta = 1$) can be represented by an inter-frame correlation γ which has value between 0 (independent) and 1 (fully dependent). As frames become separated in time, the inter-frame correlation decreases; for an inter-frame separation δ, the inter-frame correlation is γ^δ. γ could also possibly be negative if subsequent frames have inverse correlation, although this scenario is physiologically unrealistic. Frames with large inter-frame delay, $|\delta| > d$, are considered independent. Image reconstruction is then defined in terms of minimizing the augmented expression:

$$\left\| \begin{bmatrix} \mathbf{y}_{t-d} \\ \vdots \\ \mathbf{y}_t \\ \vdots \\ \mathbf{y}_{t+d} \end{bmatrix} - \begin{bmatrix} \mathbf{J} & \cdots & & & 0 \\ & \ddots & & & \\ \vdots & & \mathbf{J} & & \vdots \\ & & & \ddots & \\ 0 & \cdots & & & \mathbf{J} \end{bmatrix} \begin{bmatrix} \mathbf{x}_{t-d} \\ \vdots \\ \mathbf{x}_t \\ \vdots \\ \mathbf{x}_{t+d} \end{bmatrix} \right\|_{\tilde{\mathbf{W}}}^2 + \lambda^2 \left\| \begin{bmatrix} \mathbf{x}_{t-d} \\ \vdots \\ \mathbf{x}_t \\ \vdots \\ \mathbf{x}_{t+d} \end{bmatrix} \right\|_{\tilde{\mathbf{R}}}^2 \tag{17}$$

and (5) becomes

$$\tilde{\mathbf{B}} = \tilde{\mathbf{R}}^{-1} \tilde{\mathbf{J}}^T \left(\tilde{\mathbf{J}} \tilde{\mathbf{R}}^{-1} \tilde{\mathbf{J}}^T + \lambda^2 \tilde{\mathbf{W}}^{-1} \right)^{-1} \tag{18}$$

where $\tilde{\mathbf{W}} = \mathbf{I} \otimes \mathbf{W}$. $\tilde{\mathbf{W}}$ is diagonal since measurement noise is uncorrelated between frames. $\tilde{\mathbf{R}} = \mathbf{\Gamma}^{-1} \otimes \mathbf{R}$ where $\mathbf{\Gamma}$ is the temporal weight matrix of an image sequence $\tilde{\mathbf{x}}$ and is defined to have the form as

$$\mathbf{\Gamma} = \begin{bmatrix} 1 & \gamma & \cdots & \gamma^{2d-1} & \gamma^{2d} \\ \gamma & 1 & \cdots & \gamma^{2d-2} & \gamma^{2d-1} \\ \vdots & \vdots & \ddots & \vdots & \vdots \\ \gamma^{2d-1} & \gamma^{2d-2} & \cdots & 1 & \gamma \\ \gamma^{2d} & \gamma^{2d-1} & \cdots & \gamma & 1 \end{bmatrix} \tag{19}$$

From (18) and (19),

$$\tilde{\mathbf{B}} = \left[\mathbf{\Gamma} \otimes \left(\mathbf{P} \mathbf{J}^T \right) \right] \left[\mathbf{\Gamma} \otimes \left(\mathbf{J} \mathbf{P} \mathbf{J}^T \right) + \lambda^2 \left(\mathbf{I} \otimes \mathbf{V} \right) \right]^{-1} \tag{20}$$

Thus, (4) is rewritten as

$$\begin{bmatrix} \hat{\mathbf{x}}_{t-d} \\ \vdots \\ \hat{\mathbf{x}}_t \\ \vdots \\ \hat{\mathbf{x}}_{t+d} \end{bmatrix} = \tilde{\mathbf{B}} \tilde{\mathbf{y}}_t \tag{21}$$

Although this estimate is an augmented image sequence, we are typically only interested in the current image $\hat{\mathbf{x}}_t$. which is calculated from $\hat{\mathbf{x}}_t = \tilde{\mathbf{B}}_d \tilde{\mathbf{y}}_t$ where $\tilde{\mathbf{B}}_d$ is the rows $n_M d + 1 \ldots n_M(d+1)$ of $\tilde{\mathbf{B}}$.

2.5. Noise figure

In order to compare the different image reconstruction algorithms, it is important to choose corresponding values of the hyperparameter for each algorithm. For a review of hyperparameter selection methods for EIT, refer to Graham and Adler (2006). For our application, we wish to compare the resolution and noise performance across algorithms; however, since the regularization hyperparameter implicitly controls the compromise between resolution and noise performance, we choose to control for noise performance across algorithms, and then compare the resolution. Image reconstruction noise performance may be measured with the *noise figure* (NF) parameter of Adler and Guardo (1996). Here we generalize the NF calculation to apply to any difference EIT formulation, not simply one-step Gauss Newton type algorithms.

An EIT difference measurement vector is $\mathbf{y} = \mathbf{y}_0 + \mathbf{n}_y$, where $\mathbf{y}_0$ is the deterministic underlying signal, and $\mathbf{n}_y$ is stochastic, zero mean, measurement noise. Typically, components of $\mathbf{n}_y$ are independent, but this formulation does not make this assumption. For difference EIT, $[\mathbf{y}]_i = [\mathbf{v}_2]_i - [\mathbf{v}_1]_i$, and components of $\mathbf{n}_y$ are often assumed to be equal, but this may potentially vary if the gain varies between channels. For normalized difference EIT, $[\mathbf{y}]_i = ([\mathbf{v}_2]_i - [\mathbf{v}_1]_i)/[\mathbf{v}_1]_i$, and components of $\mathbf{n}_y$ are scaled by $diag(\mathbf{v}_1)^{-1}$. Both $\mathbf{y}_0$ and $\mathbf{n}_y$ may be complex valued.

The signal to noise ratio (SNR) of the difference measurement is defined as:

$$\text{SNR}_y = \frac{E[|\mathbf{y}|]}{\sqrt{var(\mathbf{y})}} \tag{22}$$

where we approximate $E[|\mathbf{y}|] = \frac{1}{n_M} \sum |\mathbf{y}_0|$ and calculate $var(\mathbf{y}) = \frac{1}{n_M} trace \, \Sigma_n$ where Σ_n is the measurement noise covariance. n_M is the number of measured values in the EIT data frame; we divide by n_M rather than $n_M - 1$ to calculate the variance, since the noise is known to be zero mean.

This covariance may be modelled by a noise basis, $\mathbf{N}_y$ such that $\mathbf{N}_y \mathbf{N}_y^T = \Sigma_n$. For difference EIT with independent noise on each channel, this is a diagonal matrix with $[\mathbf{N}_y]_{i,i}$ equal to the noise amplitude on channel i. Using this noise basis, $var(\mathbf{y}) = \frac{1}{n_M} \|\mathbf{N}_y\|_F^2$, where $\| \cdot \|_F^2$ is the sum of each matrix element squared (Frobenius norm squared).

A general EIT reconstruction algorithm, *EIT*, reconstructs an image estimate, $\hat{\mathbf{x}}$ from measurements as $\hat{\mathbf{x}} = EIT(\mathbf{y})$. This notation is also extended to reconstruct a matrix of column concatenated images independently from a matrix of measurements. The signal to noise ratio (SNR) of the difference image is:

$$\text{SNR}_x = \frac{E[|\mathbf{x}|]}{\sqrt{var(\mathbf{x})}} \tag{23}$$

where we approximate $E[|\mathbf{x}|] = \sum \mathbf{A} |\mathbf{x}_0|$ where $\mathbf{x}_0 = EIT(\mathbf{y}_0)$ and $\mathbf{A}$ is a diagonal matrix of the volume (or area in 2D) of each reconstructed image element. We calculate $var(\mathbf{x}) = trace \, \mathbf{A}^2 \Sigma_x$ where Σ_x is the image noise covariance. For difference EIT, image

reconstruction is linear for small $\mathbf{y}$, Using noise basis, $\mathbf{N}_x$, we calculate $\Sigma_x = \mathbf{N}_x \mathbf{N}_x^T$ where $\mathbf{N}_x = EIT(\mathbf{N}_y)$ for small $\mathbf{N}_y$, and $var(\mathbf{x}) = \|\mathbf{A}\mathbf{N}_x\|_F^2$.

The NF is the ratio of output to input SNR, where the input signal $\mathbf{y}_0$ is chosen to be a small change in a central inner circular disk covering 10% of the medium diameter, and $\mathbf{N}_n$ is scaled to be within the linear range of the algorithm.

$$\text{NF} = \frac{\text{SNR}_x}{\text{SNR}_z} = \frac{\sum \mathbf{A}\,|EIT(\mathbf{y}_0)|}{\sum |\mathbf{y}_0|} \sqrt{\frac{\|n_M \mathbf{N}_y\|_F^2}{\|\mathbf{A}\,EIT(\mathbf{N}_y)\|_F^2}} \tag{24}$$

While the SNR is normally defined in terms of the signal power, here we define it in terms of absolute amplitude. This is necessary because it is the signal amplitude, and not the power, that is spread across image elements with changes in hyperparameter; our experiments with the signal power definition do not show stable or useful results. Finally, in distinction to the definition in Adler and Guardo (1996), we calculate the absolute amplitude of the signal, allowing this definition to be appropriate to EIT systems which measure complex signals.

3. Results

Numerical simulations were conducted using a planar 2D FEM model with 5184 elements using the EIDORS software (Adler and Lionheart, 2006). A unit radius circular medium with 16 electrodes using adjacent stimulation and measurement pattern is simulated, in which a non-conductive spherical object with 0.05 unit radius rotates clockwise along a trajectory that has a radius of 2/3 unit, moving at a speed of one rotation per 40 frames. The noise performance of the algorithms was tested by adding pseudo random, zero mean Gaussian noise. All reconstructed images in figure 1 and 2 used the same random seed; tests with different seed values did not vary significantly. Images were reconstructed on a 576 element mesh, which differs from the simulation model to avoid the *inverse crime*.

Reconstructed images were calculated for four image algorithms and are shown in corresponding columns in Figs. 1 and 2: 1) *Gauss-Newton*, 2) *GN* with weighted data, 3) *temporal solver* and 4) *Kalman* filter. In each image, the position of the target at all data frames used in the algorithms are shown. In all cases, the target was at $(x, y) = (-\frac{2}{3}, 0)$ in the image shown. We explored the behaviour of these algorithms as a function of regularization hyperparameter for both noise free and noisy data. In order to choose a hyperparameter to allow comparison across algorithms, we select its value for each algorithm in order to give a fixed NF value (section 2.5). Figure 2 shows reconstructed images for a low hyperparameter value (giving $NF = 2.0$), while figure 1 shows images for a higher value (giving $NF = 0.1$). Noise levels were chosen heuristically in order to illustrate the algorithm noise performance.
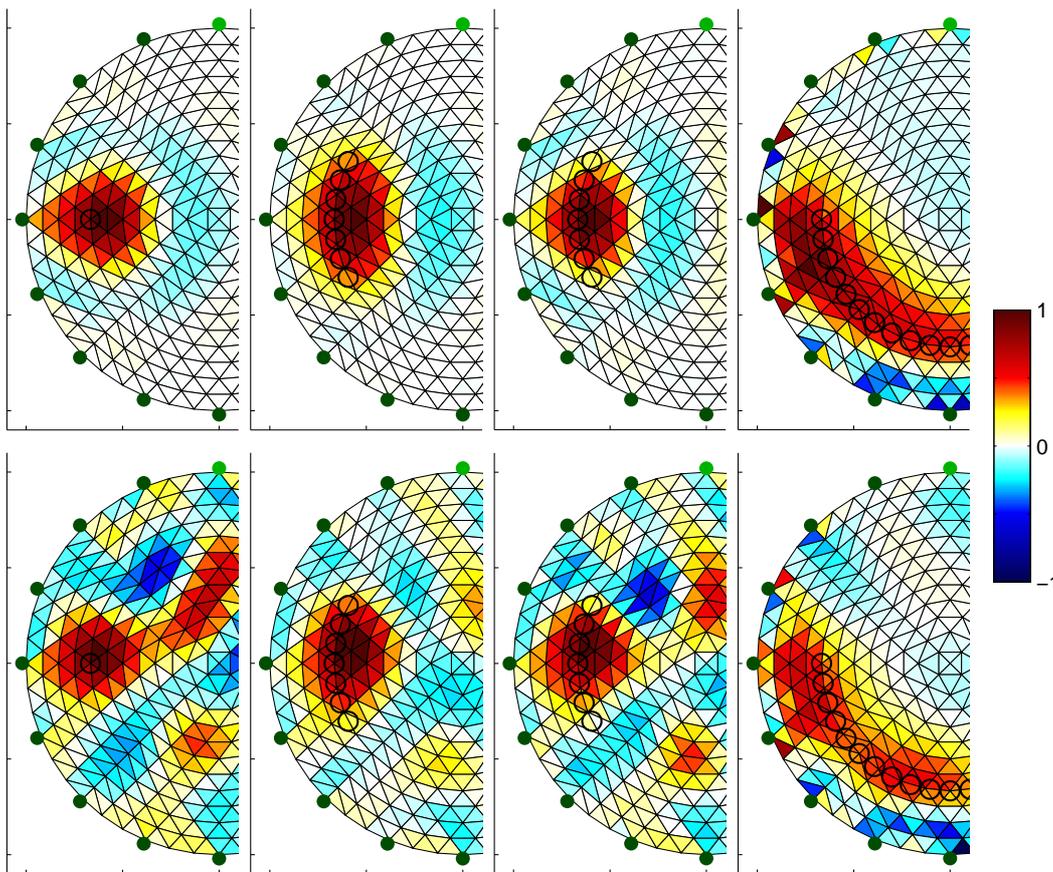
Figure 1. Reconstructed images of a target at $(-\frac{2}{3}, 0)$ for high hyperparameter (parameters $NF = 0.1$, $\gamma = 0.8$ and $d = 3$). *Top row:* No noise; *Bottom row:* $SNR = 0.25$ Each column uses a different reconstruction algorithm: *A*: Gauss-Newton *B*: Gauss-Newton with weighted data *C*: Temporal Solver *D*: Kalman Filter. The black circles in the images indicate the position of the simulated target in each data frame used for in the image reconstruction. The colourbar (with normalized units) is shown at right.

4. Discussion

Traditionally, EIT reconstruction algorithms assume each data frame to be independent. However, since EIT is able to make measurements at high frame rates, we know *a priori* that image frames are correlated. This paper addresses reconstruction of EIT data for temporal reconstructions, in which we use temporal correlations to improve reconstructed image SNR. A new *temporal reconstruction algorithm* is introduced, which directly formulates the temporal inverse in terms of a single regularized expression. We compare four different algorithms: one-step *GN* (with no temporal behaviour), *GN* with weighted data, Kalman filter reconstruction, and the proposed *temporal* reconstruction.

Results show that the *GN* algorithm is able to accurately reconstruct the position and shape of the target, but shows poorer noise performance than the other algorithms.
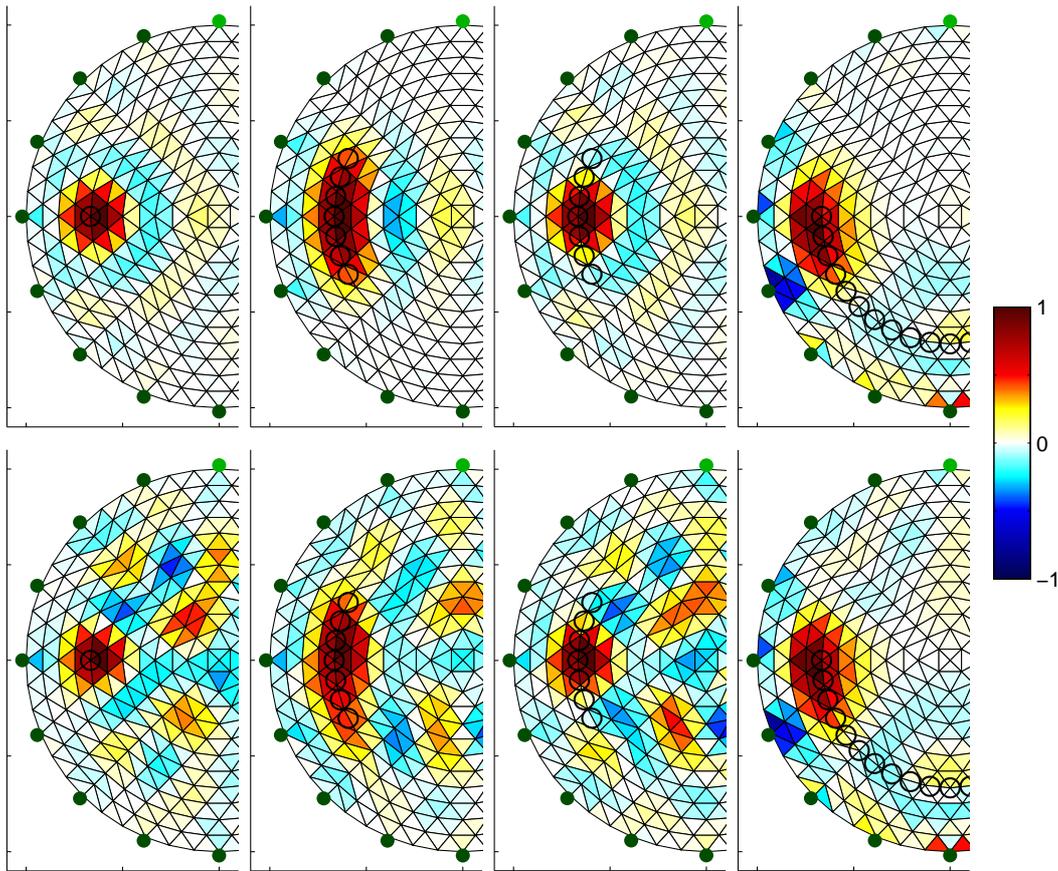
Figure 2. Reconstructed images of a target at $(-\frac{2}{3}, 0)$ for low hyperparameter (chosen for $NF = 2.0$, $\gamma = 0.8$ and $d = 3$). *Top row:* No noise; *Bottom row: SNR = 4.0* Each column uses a different reconstruction algorithm: *A*: Gauss-Newton *B*: Gauss-Newton with weighted data *C*: Temporal Solver *D*: Kalman Filter. The black circles in the images indicate the position of the simulated target in each data frame used for in the image reconstruction. The colourbar (with normalized units) is shown at right.

As the hyperparameter increases (figure 1), *GN* images tend to image targets closer toward the centre of the body. This effect is well understood for EIT (eg. Adler and Guardo, 1996), and is probably a consequence of the prior weighting of central image elements. The *GN* with averaged data blurs the reconstructed image across all the averaged data frames, but is able to show improved noise performance, as is expected from ensemble averaging. Thus, *GN* algorithms are recommended when noise levels are low, and *GN* with weighted data is a good solution when the conductivity is changing slowly with respect to the frame rate.

At low hyperparameter, the Kalman filter tends to reconstruct images with the target "pushed" outward toward the boundary, and create image artifacts and image noise on the boundary. We hypothesize that this effect is due to the iterative calculation of the error covariance term (in (12)), which results in a $\mathbf{C}^-$ which tends toward the

identity matrix. In the Kalman formulation, this term takes the place of $\mathbf{R}$ in the *GN* inverse, making the Kalman filter images resemble *GN* images with zero-order Tikhonov regularization. For larger hyperparameter values (figure 1), Kalman filter images tend to show a "trail" as a larger weighting is given to previous frame data in the current image calculation.

At high hyperparameter values, the *temporal* reconstruction shows improved resolution (illustrated as figure 1). While at low hyperparameter, it gives similar images to that of *GN* (illustrated as figure 2). This behaviour may be understood, since at low hyperparameter ($\lambda \approx 0$), (20) approximates

$$\tilde{\mathbf{B}} \approx \left[\mathbf{\Gamma} \otimes \left(\mathbf{PJ}^T\right)\right] \left[\mathbf{\Gamma} \otimes \left(\mathbf{JPJ}^T\right)\right]^{-1} = \mathbf{I} \otimes \left[\mathbf{PJ}^T \left(\mathbf{JPJ}^T\right)^{-1}\right] \qquad (25)$$

which will reconstruct each data frame independently. On the other hand, at high hyperparameter, the reconstructed image will weigh data frames together, as per *GN* with weighted data,

$$\tilde{\mathbf{B}} \approx \left[\mathbf{\Gamma} \otimes \left(\mathbf{PJ}^T\right)\right] \left[\lambda^2 \left(\mathbf{I} \otimes \mathbf{V}\right)\right]^{-1} = \mathbf{\Gamma} \otimes \left[\mathbf{PJ}^T \left(\lambda^2 \mathbf{V}\right)^{-1}\right] \qquad (26)$$

In this paper, the temporal weight γ is chosen heuristically; however, objective selection of γ is possible; its value could be estimated from the covariance of data frames measured.

In summary, this paper proposes a *temporal* EIT reconstruction algorithm. For low noise solutions (low hyperparameter) its behaviour is approximates that of Gauss-Newton reconstruction, while for high noise level and high frame rates cases where large hyperparameters are adopted, it is advantageous by reconstructing higher resolution images. It improves over Kalman filter based algorithms by allowing an explicit control over the regularization prior and the weighting of measured data. We recommend the temporal algorithm for cases in which the data noise is high and the underlying conductivity changes are rapid with respect to the frame rate.

Acknowledgments

References

Adler A, Lionheart W R B 2006, Uses and abuses of EIDORS: An extensible software base for EIT *Physiol. Meas.* **27** S25–S42

Adler A, Guardo R 1996 Electrical impedance tomography: regularized imaging and contrast detection *IEEE Trans. Med. Imaging* **15** 170–179

Cheney M, Isaacson D, Newell J C, Simske S and Goble J C 1990 NOSER: an algorithm for solving the inverse conductivity problem *Int.J.Imaging Syst.Technol.* **2** 66–75

Eichenwald E C, Stark A R 1999 High frequency ventilation: Current Status *Pediatric Review* **20** 127–133

Graham B M, Adler A 2006 Objective selection of hyperparameter for EIT *Physiol.Meas.* **27** S65–S79

Kim B S, Kim K Y, Kao T-J, Newell J C, Isaacson D, Saulnier G J 2006 Dynamic electrical impedance imaging of a chest phantom using the Kalman filter *Physiol. Meas.* **27** S81–S91

Kim K Y, Kim B S, Kim M C, Kim S 2004, Dynamic inverse obstacle problems with electrical impedance tomography *Mathematics and Computers in Simulation* **66** 399–408

Kohler B-U, Hennig C, Orglmeister R 2002 The principles of software QRS detection *IEEE Eng Med Biol Magazine* **21** 42–57

Trigo F C, Gonzalez-Lima R, Amato M B P A 2004 Electrical Impedance Tomography Using the Extended Kalman Filter *IEEE Trans Biomed Eng* **51** 72–81

Vauhkonen M Karjalainen P A Kaipio J P 1998a A Kalman filter approach to track fast impedance changes in electrical impedance tomography *IEEE Trans. Biomed. Eng.* **45** 486–493.

Vauhkonen M, Vadàsz D, Karjalainen P A, Somersalo E, Kaipio J P 1998b Tikhonov regularization and prior information in electrical impedance tomography, *IEEE Trans Med Imaging* **17** 285–293.

Wilkinson A J, Randall E W, Cilliers J J, Durrett D R, Naidoo T, Long T 2005 A 1000-measurement frames/second ERT data capture system with real-time visualization *IEEE Sensors Journal* **5** 300–307

Wolf G K, Arnold J H 2005 Noninvasive assessment of lung volume: Respiratory inductance plethysmography and electrical impedance tomography. *Critical Care Medicine* **33** S163–S169